

# Robust multi-objective optimization under multiple-uncertainties using CM-ROPAR approach: case study of the water resources allocation in the Huaihe River Basin

Jitao Zhang<sup>1,2,3</sup>, Dimitri Solomatine<sup>2,3,4</sup>, Zengchuan Dong<sup>1</sup>

<sup>1</sup>College of Hydrology and water resources, Hohai University; Nanjing, 210000, China.

<sup>2</sup>Water Resources Section, Delft University of Technology; Delft, 2628 CD, Netherlands.

<sup>3</sup>IHE Delft Institute for Water Education; Delft, 2628 AX, Netherlands

<sup>4</sup>Water Problems Institute of RAS, Moscow 119333, Russia

*Correspondence to:* Zengchuan Dong (zcdong@hhu.edu.cn)

**Abstract.** Water resources managers need to make decisions in a constantly changing environment because the data relating to water resources is uncertain and imprecise. The Robust Optimization and Probabilistic Analysis of Robustness (ROPAR) algorithm is a well-suited tool for dealing with uncertainty. Still, the failure to consider multiple uncertainties and multi-objective robustness hinder the application of the ROPAR algorithm to practical problems. This paper proposes a robust optimization and robustness probabilistic analysis method that considers numerous uncertainties and multi-objective robustness for robust water resources allocation under uncertainty. The Copula function is introduced for analyzing the probabilities of different scenarios. The robustness with respect to the two objective functions is analyzed separately, and the Pareto frontier of robustness is generated. The relationship between the robustness with respect to the two objective functions is used to evaluate water resources management strategies. Use of the method is illustrated on a case study of water resources allocation in the Huaihe River Basin. The results demonstrate that the method opens a possibility for water managers to make more informed uncertainty-aware decisions.

## 1. Introduction

Water resources is a natural resource necessary for human survival (Chen et al., 2017) but also a driving force for social and economic development (Dong and Xu, 2019). Due to the increasing population and rapid growth of economy, a contradiction between the supply and demand of water resources is becoming more acute, water quality problems are becoming more prominent, and water resources have gradually become a bottleneck for socio-economic development (Zhuang et al., 2018). This phenomenon is particularly evident in rapidly urbanizing and vital agricultural and industrial production watersheds (Yang et al., 2017). In this category of watersheds, agricultural and industrial production pose a massive challenge to water resource management (WRM) due to accelerated urbanization and rapid socio-economic development (Sun et al., 2019). River basin managers must consider water sources in an integrated manner and decide how to allocate water resources between different water-using sectors and cities within the basin (Xiong et al., 2020).

Multi-objective optimization (MOO) is an effective method for improving water resources allocation

37 (WRA) schemes (Lu et al., 2017; Abdulbaki et al., 2017). MOO can provide decision-makers with WRA  
38 options based on their preferences for objectives, which makes it a well-suited decision-making method  
39 for WRM. Ashofteh et al. (2013) constructed a bottom-line-based multi-objective optimization model to  
40 calculate WRA schemes. Habibi Davijani et al. (2016) presented a multi-objective optimal allocation  
41 model of water resources in arid areas based on maximum socioeconomic benefits. However, WRM is  
42 not only a multi-stage and multi-objective problem but also a complex problem involving uncertainties  
43 and risk management (Yu and Lu, 2018). WRM departments often need to face decision challenges under  
44 uncertain conditions (Hassanzadeh et al., 2016; Ren et al., 2019). Climate change and human activities  
45 have led to an increase in uncertainties in rainfall and water demand in the basin and hence to uncertainty  
46 in managing water resource systems (Jin et al., 2020; Ma et al., 2020; Zhu et al., 2019). Uncertain factors  
47 may lead to the risk of water shortage in the basin, so the existing WRA schemes may not be longer  
48 applicable (Keath and Brown, 2009). Therefore, it is important to study WRA under uncertainty.

49 Previously, several methods were introduced to analyze uncertainty in WRM. Scenario building and  
50 analysis is regarded as an effective method for considering possible future events and analyzing future  
51 uncertainties (Zeng et al., 2019). The fuzzy logic theory is one of the methods to deal with uncertainty,  
52 which describes uncertainty by fuzzifying the decision variables (Nikoo et al., 2013). Two-stage  
53 stochastic programming (TSP) is also an available planning method in optimization under uncertainty  
54 (Li et al., 2020). However, these approaches do not explicitly evaluate the robustness of the WRA options,  
55 although they take into account the uncertainties in WRA.

56 Robust multi-objective optimization (RMOO) is an effective method for forming robust WRA schemes.  
57 In relation to water, RMOO was actively applied in the field of water supply system (Kapelan et al., 2005;  
58 Kapelan et al., 2006). In the last decade, RMOO has been gradually applied to other areas of WRM.  
59 Yazdi et al. (2015) and Kang and Lansey (2013) applied robust optimization to design wastewater pipes  
60 by considering uncertainties such as climate change, urbanization, and population change. Marchi et al.  
61 (2016) formed stormwater harvesting schemes under variable climate conditions using RMOO. It should  
62 be pointed out however, that in the mentioned approaches the robustness is often “hidden” into the  
63 objective function or constraints and then a common MOO problem is solved that forms a single Pareto  
64 front. This is indeed an effective method to create solution set which in a certain sense is robust. However,  
65 this approach does not explicitly show the relationship between the solution and the uncertainty variables,  
66 which prevents the decision-maker from clearly understanding the impact of uncertainty, which can  
67 influence the decision. To answer this limitation, the procedure “Robust Optimization and Probabilistic  
68 Analysis of Robustness” (ROPAR) has been developed and presented first in (Solomatine, 2012). The  
69 method will generate multiple Pareto fronts, each corresponding to a sample of uncertain variables so  
70 that the statistical characteristics of the uncertainty of the solution can be analyzed. The ROPAR has been  
71 applied in the design of urban stormwater drainage pipes (Solomatine and Marquez-Calvo, 2019) and for  
72 water quality management in water distribution (Marquez Calvo et al., 2019; Quintiliani et al., 2019).

73 To the best of our knowledge, the presented versions of the ROPAR methodology have the following  
74 limitations: (1) ROPAR method has not been applied to the field of WRA; (2) ROPAR method only  
75 considers the single source of uncertainty: if there are two sources, then the joint probability of these  
76 sources needs to be considered; (3) ROPAR method only analyses the variability of one objective under  
77 conditions where the other objective function level is fixed. Although the ROPAR method can provide  
78 decision-makers with a robust solution under certain conditions, it does not take into account the  
79 relationship between the two objective functions.

80

81

82 Based on the above analysis, although the ROPAR method has proven to be suitable for dealing  
83 with uncertainty, it still needs improvement. In this study, we propose a Copula-Multi-objective Robust  
84 Optimization and Probabilistic Analysis of Robustness (CM-ROPAR) procedure under multiple  
85 uncertainties for WRA. The proposed new procedure of the ROPAR-family considers the joint  
86 probability distribution of uncertainties (in this case, inflows) and enables decision-makers to check the  
87 robustness of the two objective functions separately.

88 The following text is structured as follows. First, the Chapter 2 presents the methodology of the  
89 paper. It mainly includes the method of Copula function, the method of CM-ROPAR algorithm, the  
90 definition of robustness and the construction of water resources allocation model. Then, the Chapter 3  
91 introduces the overview of the study area. Then, the Chapter 4 introduces the application examples of  
92 CM-ROPAR algorithm, and this paper is an example of water resources allocation of Huaihe River Basin.  
93 Finally, the last Chapter introduces the conclusion of the paper.

94

## 95 2. Methodology

### 96 2.1 Method of Copula Function

97 Sklar proposed Copula theory in 1959, in which he decomposed an N-dimensional Joint Distribution  
98 Function (JDF) into a Copula function and N Marginal Distribution Functions (MDF), which are not  
99 required to be the same distribution for N variables and can be used to describe the correlation between  
100 arbitrary variables. Nelsen gave a strict definition of Copula function in 1999 (Nelsen et al., 2008).  
101 Copula function is the function that connects the JDF with their respective MDF. Copula functions can  
102 be expressed as:

$$103 C_{\theta}(u_1, u_2 \dots u_n) = C_{\theta}[F_1(x_1), F_2(x_2) \dots F_n(x_n)] \quad (1)$$

104 where  $x_1, x_2 \dots x_n$  are random vectors,  $F_1(x_1), F_2(x_2) \dots F_n(x_n)$  are MDF of the random vectors,  
105  $\theta$  is the parameter of copula function.

106 The basic copula functions are mainly classified into Archimedean, elliptic, and quadratic types.  
107 Among them, Archimedean Copula functions have been widely applied in the field of hydrology. The  
108 most used Archimedean Copula multidimensional joint distribution models are the following:

109 (1) GH-Copula joint distribution model

$$110 C_{\theta}(u_1, u_2 \dots u_n) = \exp \left[ -(\sum_{i=1}^n (-\ln u_i)^{\theta})^{\frac{1}{\theta}} \right] \quad (\theta > 1), \quad (2)$$

111 (2) Clayton Copula joint distribution model

$$112 C_{\theta}(u_1, u_2 \dots u_n) = \left[ 1 + \sum_{i=1}^n (u_i^{-\theta} - 1) \right]^{-\frac{1}{\theta}} \quad (\theta > 1), \quad (3)$$

113 (3) Frank Copula joint distribution model

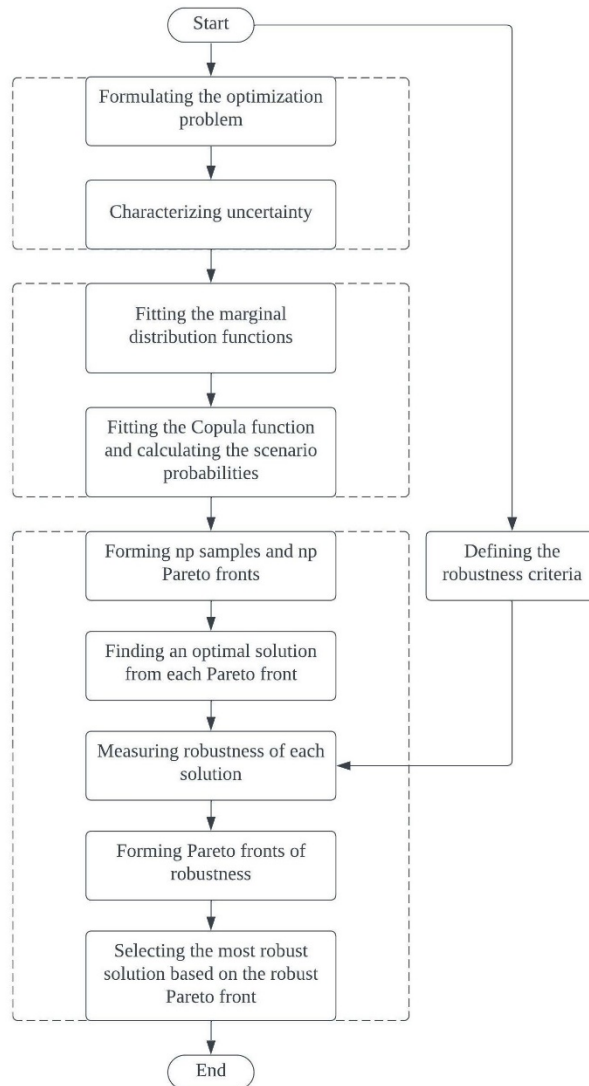
$$114 C_{\theta}(u_1, u_2 \dots u_n) = -\frac{1}{\theta} \ln \left[ 1 + \frac{\prod_{i=1}^n (e^{-\theta u_i} - 1)}{(e^{-\theta} - 1)^{n-1}} \right] \quad (\theta > 1), \quad (4)$$

115 In a river basin, there may be different drought or wet conditions between different intervals of  
116 inflow, so the probability of drought and wet encounters between different intervals of inflow needs to  
117 be investigated. According to the analysis in Section 2.1, it is known that Copula function can be used to  
118 construct the multivariate joint distribution function. Therefore, this paper adopts Copula function theory

119 to construct the joint distribution and analyze the drought and wet encounter probability. The steps of  
 120 Copula function-based wet-dry encounter analysis are as follows: 1. Fit and Select the MDF. The widely  
 121 applied probability distribution functions are mainly Pearson type 3 distribution (P-III), T-distribution,  
 122 Normal distribution, etc. 2. Fit and Select Copula distribution function. Fitting different MDF of the  
 123 runoff, using the AIC and BIC criterion for the selection of the fitted MDF. 3. Calculate the probability  
 124 of a dry and wet encounters between different interval inflows.  
 125

## 126 2.2 Method of CM-ROPAR

127 The basic flow of CM-ROPAR algorithm is shown in Figure 1. Firstly, the multi-objective optimization  
 128 problem is defined and the uncertainty variables are clarified; secondly, the Copula function is used to  
 129 analyze the relationship between the two sources of uncertainty; and finally, through sampling and multi-  
 130 objective optimization calculations, the robustness of each solution is identified and the one with the  
 131 most comprehensive robustness is selected.  
 132



133

134 **Figure 1.** Flowchart of CM-ROPAR.

135

136 The specific process of optimal water allocation under runoff uncertainty based on MROPAR algorithm  
137 is as follows.

138 **Part 1** (Analyzing the wet-dry encounters)

139 1. Analyze the inflow wet and dry encounters. If the basin has  $k$  inflows, then there are  $3^k$  wet-  
140 dry scenarios. For example, suppose there is one inflow in the upper and one in the middle reaches of the  
141 basin. In that case, there are 9 scenarios: wet-medium, wet-wet, medium-wet, medium-medium, medium-  
142 dry, dry-wet, dry-medium, and dry-dry.

143 2. Choose a scenario from 1 to  $3^k$ .

144 **Part 2** (Sampling-Inflow)

145 3. Based on the recorded annual inflow data  $Q$ , it is assumed that  $Q$  is not a definite value but

$$146 Q = i_{uncertainty} * Q, \quad (5)$$

$$147 i_{uncertainty} \sim N(\mu, \sigma^2), \quad (6)$$

148 where  $i_{uncertainty}$  follows a normal distribution.

149 4. For  $i = 1 \dots np$  do

150 5. Sample  $u$  (inflow). As mentioned before, the uncertainty variable is obtained from the normal  
151 distribution  $N(\mu, \sigma^2)$ . Assuming that the uncertainty variable follows  $N(1, 0.0025)$ , this  
152 represents that a 99.74% probability of the uncertainty variable falling within the  
153 interval  $[0.85, 1.15]$  and the inflow sample falling within the interval  $[0.85 * Q, 1.15 * Q]$ .

155 **Part 3** (Forming the optimal solution set through  $np$  Pareto fronts)

156 7. Select an ideal solution ( $IS$ ) in each Pareto front  $F_r$  based on the distance to the origin point,  
157 forming the optimal solution set (set  $S$ ).

158 **Part 4** (Evaluate the robustness of each solution)

159 8. Select a solution  $s_i$  ( $i = 1 \dots np$ ) from the solution set  $S$ .

160 9. Cast the inflow case  $u_r$  ( $r = 1 \dots np$ ) into  $s_i$  and calculate  $P_r(u_r, s_i)$  and  $WD_r(u_r, s_i)$ ,  
161 respectively, to form 1200 values of  $P_r$  and  $WD_r$  ( $r = 1 \dots np$ ).

162 10. Select the robustness evaluation criteria,  $RC1, RC2, RC3, RC4$ .

163 11. For each  $s_i$  ( $i = 1 \dots np$ ), calculate the  $RC1, RC2, RC3, RC4$  and  $SRI$  corresponding to  $P_r$   
164 and  $WD_r$  respectively. Plot the corresponding graphs and find the Pareto front of each graph.

165 12. Find the solution with the highest robustness.

166 End

## 167 2.3 Defining the robustness criteria

168 According to the general definition of robustness, four common Robustness Criteria ( $RC$ ) were used in  
169 this study (Beyer and Sendhoff, 2007). These must be minimized to achieve the maximum robustness of  
170 the solution, so the lower the criteria, the higher the robustness.

171 For the four  $RC$ , two MOO are implicitly defined, and optimization can be named Two Layer-Multi-  
172 objective optimization of Robustness Criteria (TL-MOORC). It is worth noting that TL-MOORC differs  
173 from the problem's MOO. A one-layer MOORC is a solution that may not be minimized at all four  $RC$   
174 simultaneously. This problem can be solved by aggregating the four  $RC$  into one, for example, using a  
175 linear weighted combination. The second layer of MOORC is that for the two objective functions of a  
176 solution, the  $RC$  for both objective functions may not be minimized at the same time. Therefore, a trade-  
177 off must be made between the  $RC$  for the two objective functions.

178 The first  $RC$  is the expected value of each objective function, denoted as  $RC1$ . It reflects the fact that

179 we want to find a solution that is good on average across all uncertainties and can be represented by:

$$180 \quad RC1(s) = \int_{N(s,u)} f(s, u) p(u) du, \quad (7)$$

181 Where is the probability density function of the uncertain variable  $u$ ; it is the neighborhood of the  
182 solution  $s$ .

183 The second  $RC$  is the ‘worst case’ (or ‘minimax’ case), denoted as  $RC2$ . This  $RC$  is related to  
184 robustness because we want to find a solution  $s$  such that the value of each objective function in the  
185 worst case is the minimum possible. It can be presented as follows:

$$186 \quad RC2(s) = \min \left( \max_{N(s,u)} (f(s, u)) \right), \quad (8)$$

187 The third  $RC$  is the ‘standard deviation’ of each objective function, denoted as  $RC3$ .  $RC3$  is  
188 related to the robustness of each objective function because we want to find a solution  $s$  such that the  
189 value of the objective function would not vary too much due to uncertainty. It can be expressed as follows:

$$190 \quad RC3(s) = \sqrt{\int_{N(s,u)} (f(s, u) - f(u))^2 p(u) du}, \quad (9)$$

191 The fourth  $RC$  is the "probabilistic threshold", denoted as  $RC4$ . We want to find a solution  $s$  that  
192 minimizes the probability that the objective function is higher than the threshold of interest  $q$ . This  
193 criterion is usually associated with the reliability of the system. It can be expressed as follows:

$$194 \quad RC4(s) = Pr(f(s, u) > q|s), \quad (10)$$

195 In order to evaluate the integrated robustness of the water resources allocation scheme, the weighted  
196 sum of the four Normalized  $RC$  ( $NRCi$ ) in this study was used as the integrated robustness criteria. In  
197 this study, we consider that the four  $RC$  to be of equal importance, so all four indicators are given a  
198 weight of  $\frac{1}{4}$ .

$$199 \quad SRI = \frac{1}{4}NRC1 + \frac{1}{4}NRC2 + \frac{1}{4}NRC3 + \frac{1}{4}NRC4, \quad (11)$$

200 (of course, other ways of aggregation can be considered as well.)

## 201 2.4 Construction of WRA Model

### 202 Objective function

203 (1) Social Goals: Water Deficit ( $WD$ )

$$204 \quad \min f_1(Q) = \sum_{j=1}^J \sum_{k=1}^K \left( \frac{D_{jk} - \sum_{t=1}^T \sum_{i=1}^I Q_{ijkt}}{D_{jk}} \right)^2, \quad (12)$$

205 Where  $D_{jk}$  denotes the water demand of the water consumption department  $k$  of the city  $j$ .  $Q_{ijkt}$  is the  
206 water supply quantity of water source  $i$  to water consumption department  $k$  of the city  $j$  in the period  
207  $t$ .

208 (2) Ecological goals: Pollution ( $P$ )

$$209 \quad \min f_2(Q) = \sum_{j=1}^J \sum_{k=1}^K d_{jk} p_{jk} \sum_{i=1}^I \sum_{t=1}^T Q_{ijkt}, \quad (13)$$

210 Where  $d_{jk}$  denotes the representative pollutant discharge per unit of wastewater of the water department  
211  $k$  of calculation unit  $j$  (ton/m<sup>3</sup>) and  $p_{jk}$  represents the sewage discharge coefficient of the water  
212 consumption department of calculation unit. Discharge coefficient of water consumption department  $k$   
213 of calculation unit  $j$ .  $Q_{ijkt}$  is the water supply quantity of water source  $i$  to water consumption  
214 department  $k$  of calculation unit  $j$  in the period  $t$ .

### 215 Constraints

216 (1) Water demand constraint

217  $\sum_{i=1}^I \sum_{t=1}^T Q_{ijkt} \leq D_{jk},$  (14)

218 (2) Water supply capacity constraint

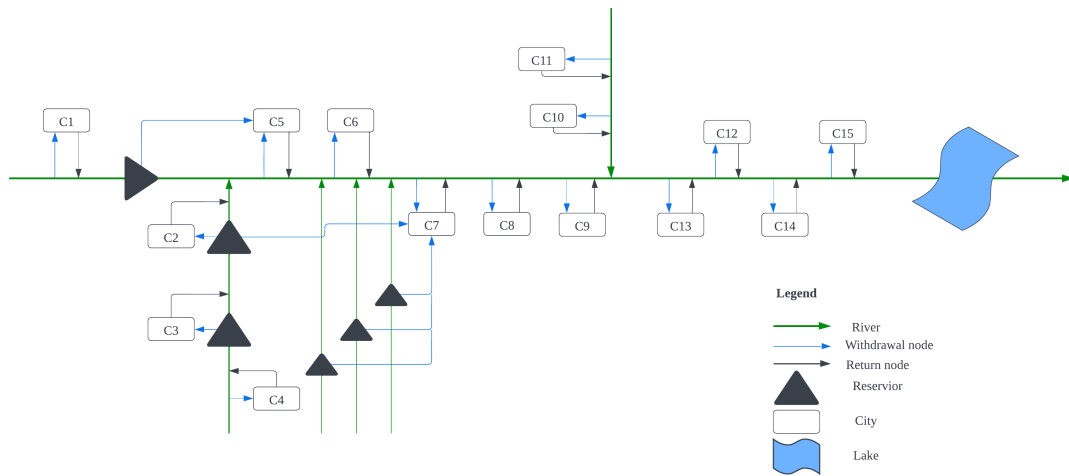
219  $\sum_{k=1}^K \sum_{j=1}^J \sum_{t=1}^T Q_{ijkt} \leq U_i,$  (15)

220 (3) Water Resources Constraint

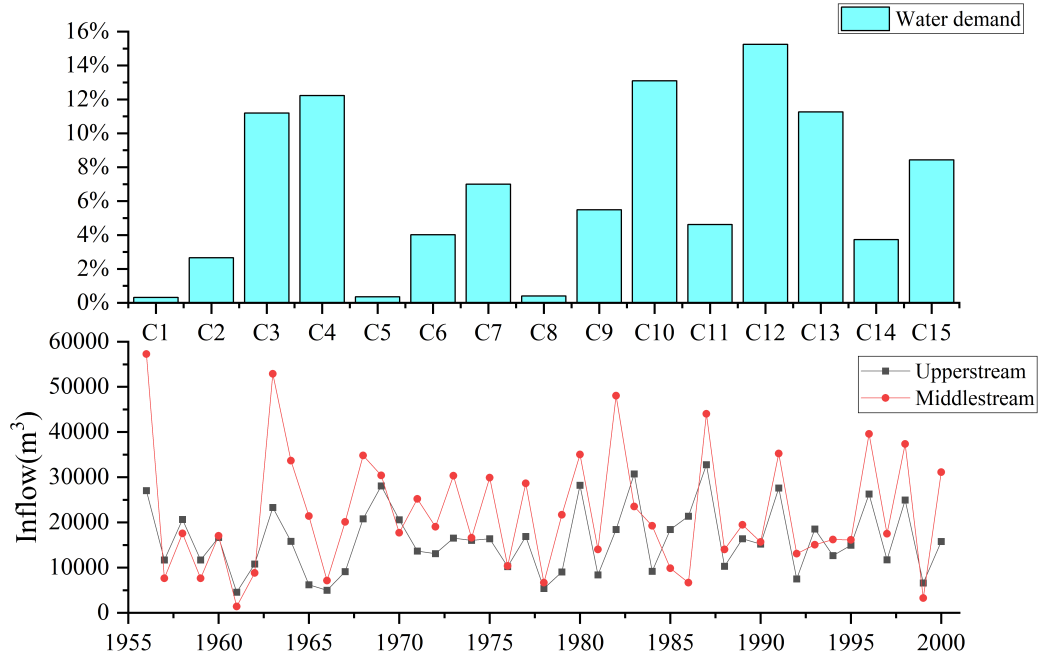
221  $\sum_{j=1}^J \sum_{k=1}^K Q_{ijk} \leq WR_i,$  (16)

222 3. Study Area Overview

223 The Huaihe River Basin is located in the eastern part of China, and as shown in Figure 2, the middle and  
 224 upper basin flows through 15 cities of Henan Province and Anhui Province. It is an important agricultural  
 225 and industrial production base in China (Xu et al., 2019). As shown in the Figure 3, the inflow of the  
 226 Huaihe River Basin varies significantly between different years and between different regions, and the  
 227 water demand is uneven among cities. In this study, water demand is calculated by using the quota  
 228 method commonly used in the field of water resources. In addition, due to the discharge of pollutants,  
 229 the contradiction between supply and demand of water resources in the middle and upper reaches of the  
 230 Huaihe River Basin has become increasingly fierce. Therefore, it is meaningful to study the optimal  
 231 allocation of water resources and propose a robust water resources allocation scheme based on the wet-  
 232 dry encounters in the Huaihe River Basin.



233  
 234 **Figure 2.** Overview of watershed water supply.



235

236 **Figure 3.** Water demand proportion and inflow historical data.

237 4. Results and discussion

238 4.1 Identification of marginal distribution functions

239 According to the first part (step 1-2) of the CM-ROPAR process, we need to construct the joint  
 240 probability distributions for the upstream and midstream inflow and generate nine inflow scenarios via  
 241 the Copula function. Therefore, before constructing the JDF, we need to construct the MDF for the  
 242 upstream and midstream inflows respectively. Based on the Kolmogorov-Smirnov (K-S) test results, we  
 243 found that the best-fitting distributions for the upstream and midstream were the Weibull and P-III  
 244 distributions, respectively.

245 4.2 Analysis of upstream and midstream dry and wet encounters

246 The optimal Copula function is selected by comparing the Akaike information criterion (AIC) and the  
 247 Bayesian information criterion (BIC), AIC and BIC values in Table 1. It can be concluded that the joint  
 248 distribution function of the upper and middle reaches of the Huaihe River Basin is consistent with the  
 249 joint distribution of the Clayton Copula function.

250

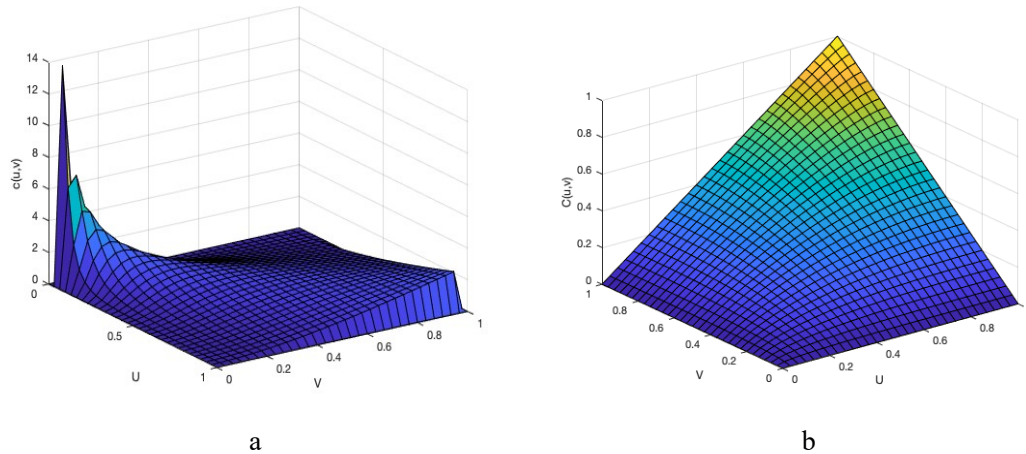
251 **Table 1.** AIC and BIC values for Copula functions.

	Gaussian	t	Clayton	Gumbel	Frank
AIC	-20.86	-18.34	<b>-22.69</b>	-12.47	-20.03
BIC	-19.06	-14.73	<b>-20.88</b>	-10.67	-18.22

252

253 Substituting the multi-year annual inflow for the upper and middle reaches of the Huaihe River Basin  
 254 into the Clayton Copula function, respectively, the following results were obtained.





255 **Figure 4.** Clayton Copula function.

256

257 As shown in Figure 4, the joint distribution of the annual incoming water in the upper and middle reaches  
 258 of the Huaihe River Basin has symmetry. In addition, the joint distribution of annual water in the upper  
 259 and middle reaches has a tail correlation, which indicates a higher probability of simultaneous wetness  
 260 or drought in the upper and middle reaches.

261

262 **Table 2.** The probabilities of 9 scenarios.

Wet and Dry encounters/%		Upstream		
		Wet	Medium	Dry
Middlestream	Wet	27.7	7.8	5.3
	Medium	11.6	6.5	4.6
	Dry	4.6	7.8	24.1

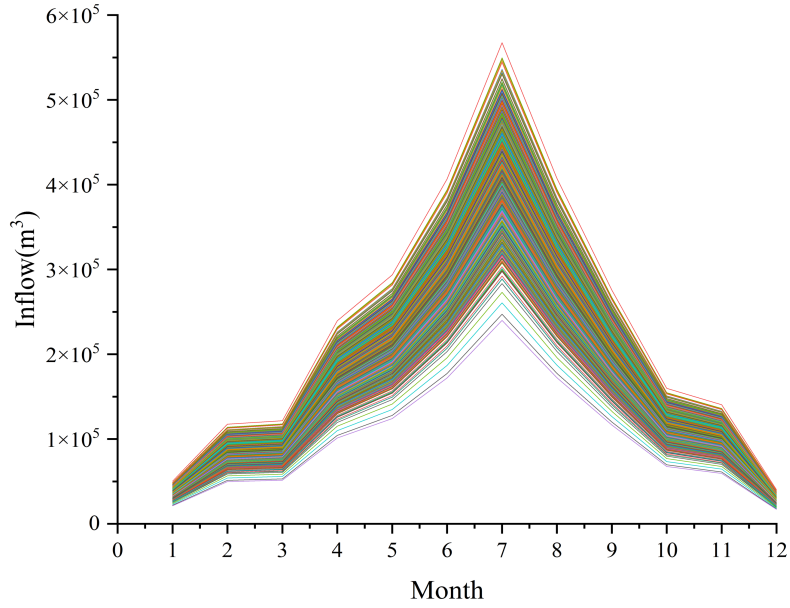
263

264 As shown in Table 2, the probability of drought-wetness synchronization in the upper and middle reaches  
 265 of the Huaihe River Basin is 58.3%, while the probability of asynchrony is 41.7%. The former is 16.6%  
 266 higher than the latter, indicating that the upper and middle reaches are less able to complement each other.  
 267 The joint distribution has a maximum probability of 27.7% that the upstream and midstream are both  
 268 wet, and the risk of water scarcity is minimal under this scenario. The joint distribution has the second-  
 269 highest probability of both upstream and midstream being dry at 24.1%, with the highest risk of water  
 270 scarcity under this scenario.

### 271 **4.3 Considering solutions for the uncertainty of inflow through MROPAR**

272 In this study the situation when the upper and middle reaches are both wet is considered as a case study.  
 273 For deterministic optimization we opted for the NSGA-II algorithm, which is widely used and has good  
 274 historical performance (Reed et al., 2013). Inflow uncertainty is modelled by sampling 1200 inflows, as  
 275 shown in Figure 5. In this study, NSGA- II algorithm is used for multi-objective function  
 276 solving. For algorithm parameterization, the population size is 100, generation is 1000,  
 277 cross rate is 0.9 and mutate rate is 0.2.

278

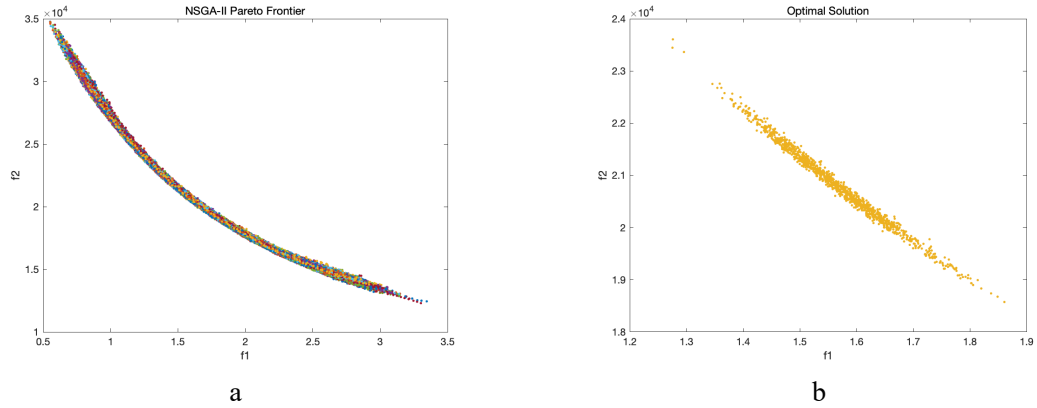


279

280 **Figure 5.** Inflow samples.

281

282 Figure 6(a) shows that 1200 Pareto fronts calculated for each sampled inflow, through steps 3-6 of CM-  
 283 ROPAR. Figure 6(b) shows 1200 ideal solutions  $s$ , selected based on their distance to the ideal solution  
 284 (step 7 of CM-ROPAR).



285

**Figure 6.** a: 1200 Pareto fronts (f1: water deficit; f2: pollution) and b: 1200 ideal solutions (f1: water  
 286 deficit; f2: pollution) selected based on their distance to the ideal solution.

287

#### 4.4 Assessing robustness of the solutions found by CM-ROPAR

288

Four robustness criteria are calculated for each solution  $s$  in the solution set  $S$ . Given the solution  $s$   
 289 to be evaluated, it is necessary to calculate  $WD(s, IF_r)(r = 1 \dots np)$  and  $P(s, IF_r)(r = 1 \dots np)$  in  
 290 order to calculate the four robustness criteria, where  $IF_r$  is the  $r$ th sample of inflow.  $r$  depends on  
 291 the number of samples; in this study, 1200 samples were taken, so  $np$  is 1200.

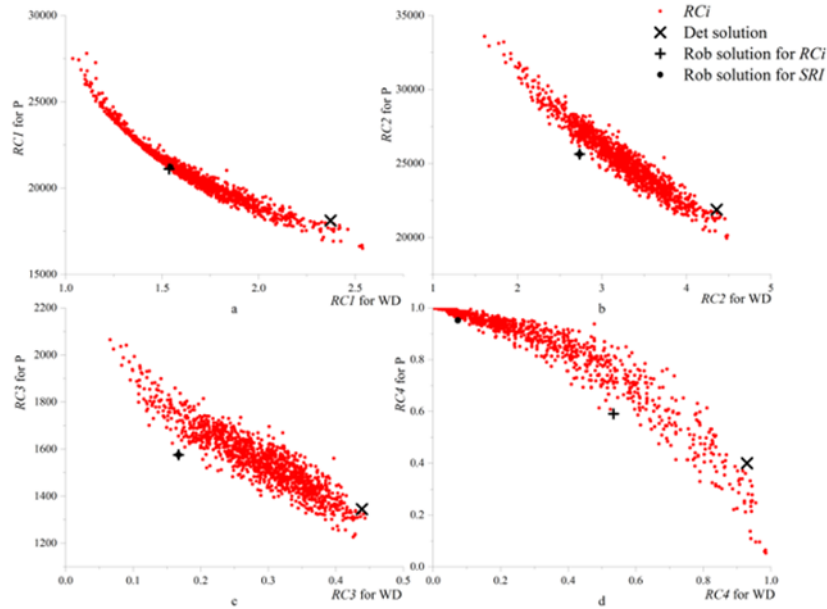
292

As shown in Table 3 and Figure 7,  $RC1, RC2, RC3, RC4$  and  $SRI$  for  $WD$  and  $P$  can be  
 293 calculated for each solution in  $S$ , and the solutions corresponding to the smallest value in each  $RCi$  and  
 294 the solutions corresponding to the smallest value in  $SRI$  can be identified, respectively. In addition, we  
 295 also feed 1200 samples to the deterministic solution and calculate  $RC1, RC2, RC3, RC4$  and  $SRI$  for  
 296  $WD$  and  $P$ .

297

**Table 3.** Optimal solution numbers for different robustness criteria.

	$RC1$	$RC2$	$RC3$	$RC4$	$SRI$
$WD$	535	361	361	361	361
$P$	876	876	876	876	876
$IS$	629	84	84	915	84



299

300 **Figure 7.** Performance of the robustness of solutions (a:  $RC1$ , b:  $RC2$ , c:  $RC3$ , d:  $RC4$ ): robust model  
 301 solutions (red dots), deterministic model solution (black  $\times$ ), solution closest to origin for  $RCi$  (black +),  
 302 solution closest to origin for  $SRI$  (black dot). The horizontal axis represents the performance of the  
 303 robustness for  $WD$ . The vertical axis represents the robustness performance for  $P$ .

304

305 Figure 7 shows the performance of 1200 robust model solutions (red dots) and one deterministic model  
 306 solution (black  $\times$ ), for the four robustness criteria. From Figure 7, four Pareto fronts can also be found,  
 307 which indicate the competitive relationship between water deficit and pollution emissions for each  
 308 robustness criterion dimension. As shown in Figure 7(a), we can observe an interesting phenomenon that  
 309 the left-most extreme solution (red dot) has the smallest robustness index  $RC1$  for water deficit, but the  
 310 highest robustness index  $RC1$  for pollution; the right-most extreme solution (red dot) has the largest  
 311 robustness index  $RC1$  for water deficit, but the smallest robustness index  $RC1$  for pollution. Similarly,  
 312 this phenomenon can be also observed for the robustness criteria  $RC2$ ,  $RC3$ , and  $RC4$ . More  
 313 importantly, as shown in Table 3, the extreme solutions and the solutions closest to the origin point may  
 314 differ for different robustness criteria. Specifically, for  $RC1$ , solution No. 535 is the most robust for  
 315 water deficit, and solution No. 876 is the most robust for pollution; for  $RC2$ ,  $RC3$ , and  $RC4$ , the most  
 316 robust solution for water deficit is solution No. 361, and the most robust solution for pollution is solution  
 317 No. 876.

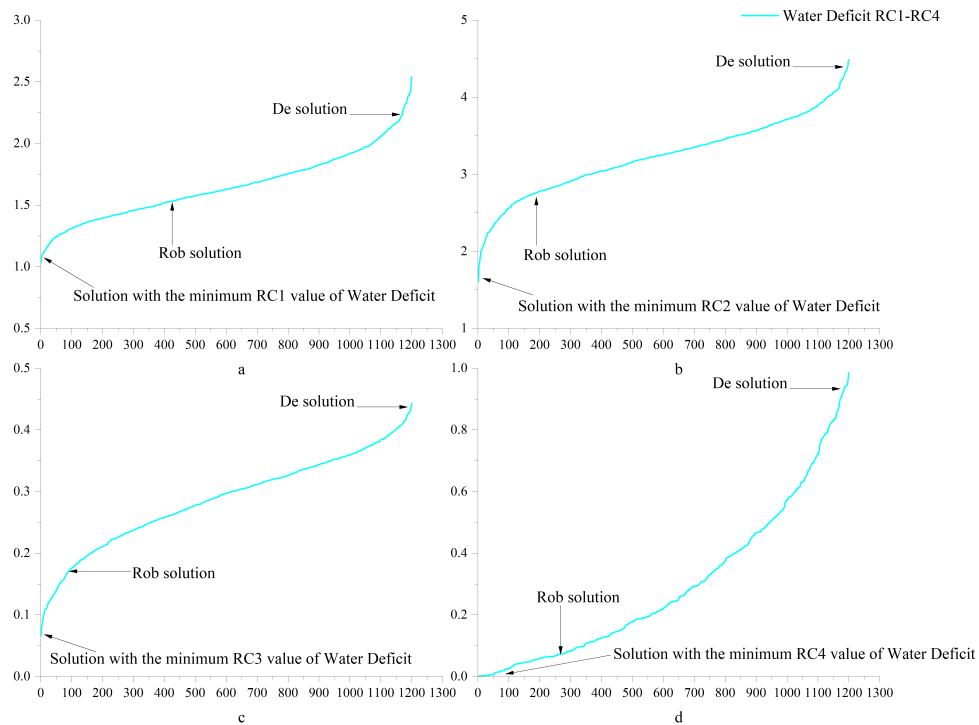
318

319 Because there are many non-inferior solutions in the Pareto frontier, the decision-makers must  
 320 choose among them. The decision-makers need not only to choose among the non-inferior solutions but  
 321 also to evaluate the trade-off between different robustness criteria or to choose the best one by combining  
 the criteria. This study takes the distance to the origin as the basis for such choice. As shown in Table 3,

322 for  $RC1$ ,  $RC2$ ,  $RC3$ , and  $RC4$ , the closest points to the origin are solution No. 629, solution No. 84,  
 323 and solution No. 915, respectively.

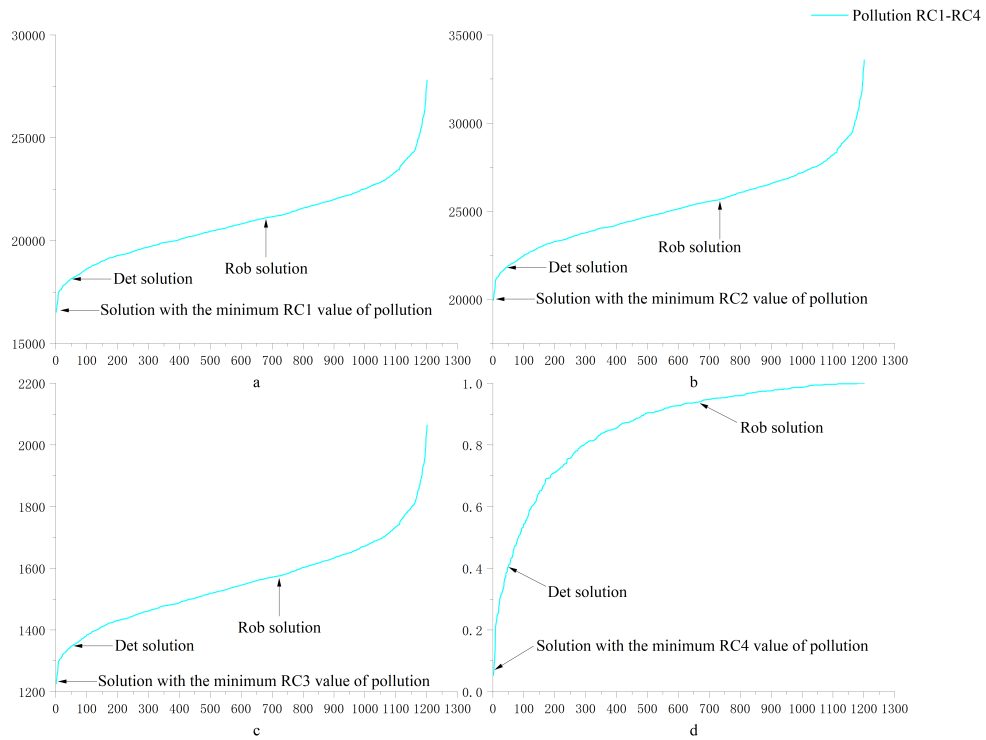
#### 324 4.5 Comparing solutions found by deterministic and robust approaches

325 To see a more general relationship between the 1201 solutions (i.e., 1200 from the robust optimization  
 326 solution and 1 from the deterministic optimization solution), the performance of each solution for water  
 327 deficit and pollution on each of the four robustness criteria (sorted from smallest to largest) is plotted in  
 328 Figure 8 and Figure 9.



329 **Figure 8.** Robustness of water deficit (a:  $RC1$ , b:  $RC2$ , c:  $RC3$ , d:  $RC4$ ). The horizontal coordinate  
 330 represents the number of solutions and the vertical coordinate represents the robustness of the solution.  
 331

332  
 333 As shown in Figure 8, for water scarcity, the robust solution performed significantly better than the  
 334 deterministic solution. Specifically, for the four robustness criteria, the robust solution outperforms  
 335 63.1%, 85.6%, 92.7%, and 77.7% of the solutions, respectively, while the deterministic solution  
 336 outperforms only approximately 1% of the solutions. To analyze the robust and deterministic solutions  
 337 more accurately and intuitively, this study applied the ratio of  $RC(Det)/RC(Rob)$  to compare the  
 338 robustness of the two solutions. The ratios of  $RC(Det)/RC(Rob)$  are 1.53, 1.59, 2.62, and 12.67 in the  
 339 four robustness criteria dimensions. This means that, regarding water deficit, the deterministic model  
 340 solution may lead to 53%, 59%, 162%, and 1167% more variability in the four robustness criteria  
 341 dimensions.

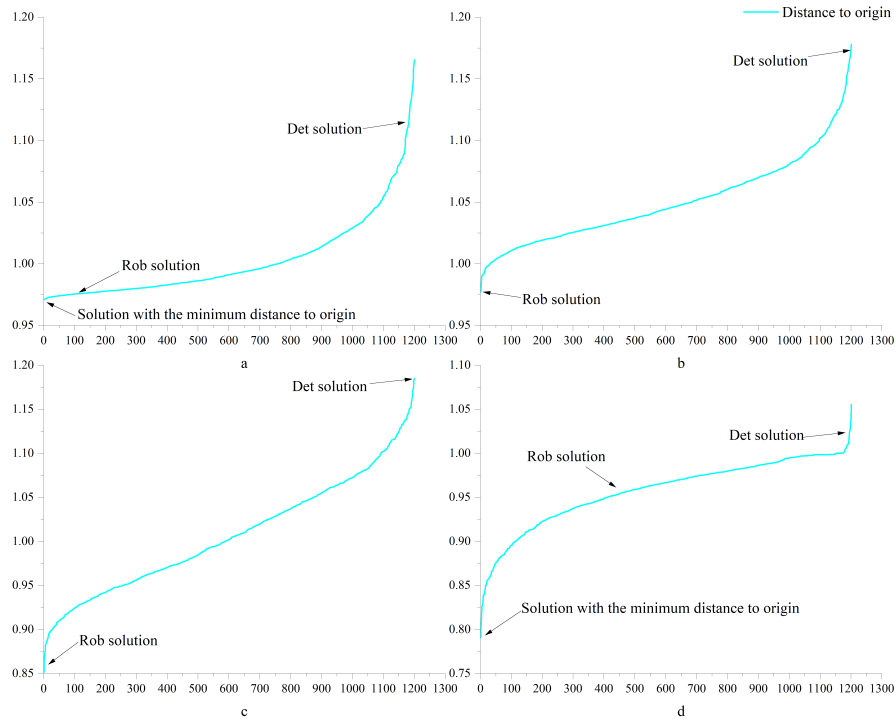


342

343 **Figure 9.** Robustness of pollution (a:  $RC1$ , b:  $RC2$ , c:  $RC3$ , d:  $RC4$ ). The horizontal coordinate  
 344 represents the number of solutions and the vertical coordinate represents the robustness of the solution.

345

346 However, as shown in Figure 9, the deterministic solution slightly outperforms the robust solution for  
 347 pollution. Specifically, for the four robustness criteria, the deterministic solution outperforms 96% of the  
 348 solutions, respectively, while the robust solution outperforms about 40% of the solutions. Similarly, we  
 349 compare the two solutions by the ratio of  $RC(Rob)/RC(Det)$ . We find that the  $RC(Rob)/RC(Det)$   
 350 ratio is about 1.17 for  $RC1$  to  $RC3$  and 2.37 for  $RC4$ . This means that, in terms of pollution, the robust  
 351 solution may lead to 17% more variability for  $RC1$  to  $RC3$  and 137% more variability for  $RC4$ .

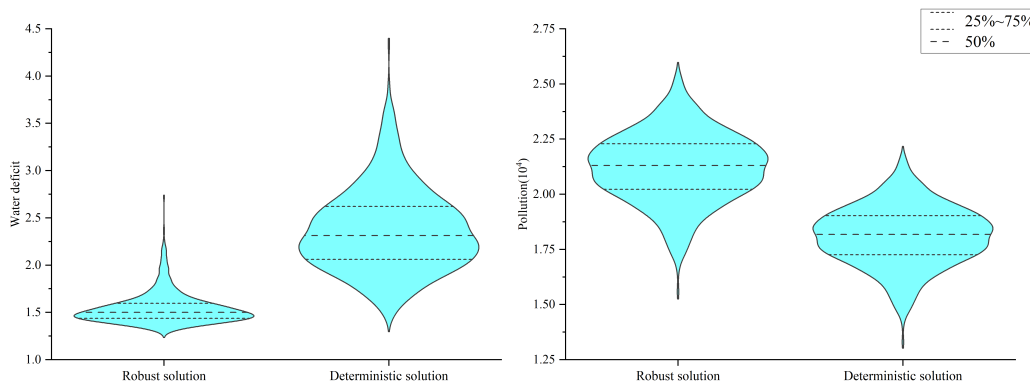


352

353 **Figure 10.** Comprehensive robustness for four indicators (a:  $RC1$ , b:  $RC2$ , c:  $RC3$ , d:  $RC4$ ). The  
 354 horizontal coordinate represents the number of solutions and the vertical coordinate represents the  
 355 robustness of the solution.

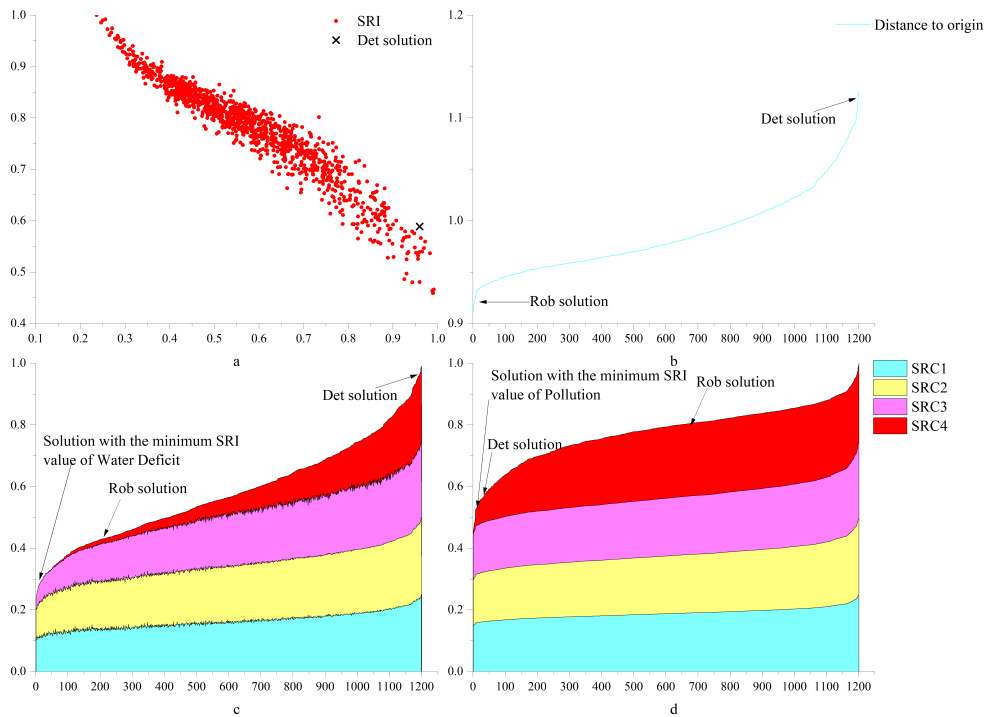
356

357 In order to analyze the comprehensive performance of each solution, rather than just the robustness of a  
 358 single objective, this study reflects the comprehensive implementation of each solution in terms of the  
 359 distance from the solution to the origin. As shown in Figure 10, the comprehensive performance of the  
 360 robust solution for  $RC1$  to  $RC4$  is significantly better than that of the deterministic model solution.  
 361 Specifically, the robust solution outperforms 90.3% and 62.2% of the solutions in  $RC1$  and  $RC4$ ,  
 362 respectively, and outperforms all solutions in  $RC2$  and  $RC3$ , while the deterministic solution performs  
 363 exceptionally poorly in all four robustness criteria. According to the ratio of  $Dis(Rob)/Dis(Det)$ , we  
 364 can find that the robust solution is 16.8%, 19.8%, 39.2%, and 7.3% more robust than the deterministic  
 365 solution in the four robustness dimensions, respectively.



366

367 **Figure 11.** The integrated robustness index distribution of the robust and deterministic solution.



368

369 **Figure 12.** Comprehensive robustness criteria performance (a: Performance of comprehensive  
 370 robustness criterion, b: Comprehensive robustness of robust solutions and deterministic solution, c and  
 371 d: comprehensive robustness criteria for water deficit and pollution).

372

373 As shown in Figure 11, for water scarcity, the integrated criteria of the robust solution is clustered at  
 374 approximately 0.5 and is significantly more robust than the deterministic solution; for pollution, the  
 375 integrated index of the robust solution is significantly higher than that of the deterministic solution, but  
 376 the span of the integrated index of the two solutions is similar, so the robustness of the deterministic  
 377 solution is slightly better than that of the robust solution.

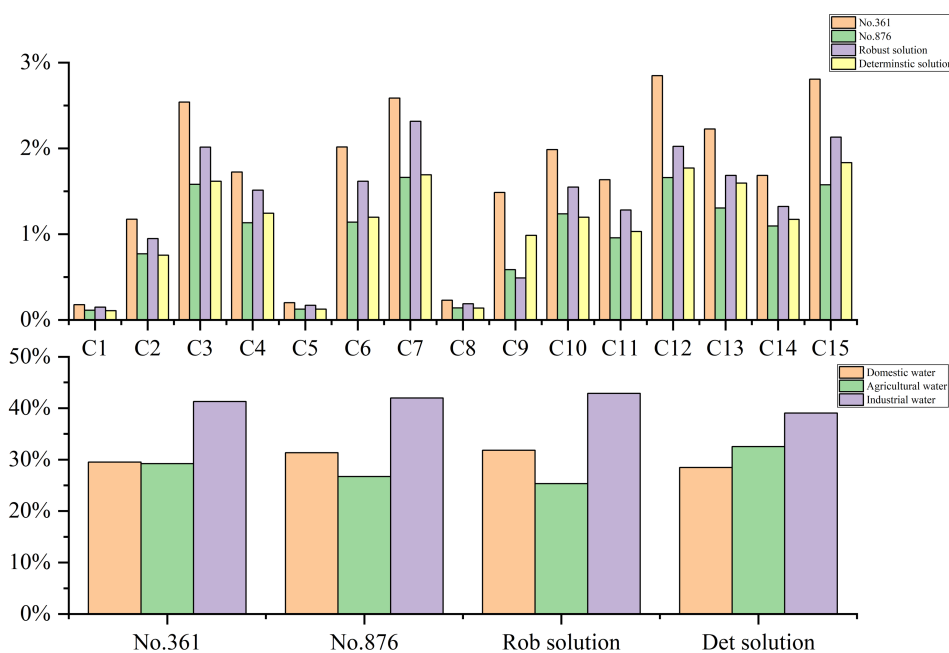
378 Similarly, as shown in Figure 12, there is also a Pareto front for the composite robustness criteria. For  
 379 water deficit, the robustness of the robust solution is better than the deterministic solution; for pollution,  
 380 the robustness of the deterministic solution is better than the robust solution. Specifically, for water deficit,  
 381 the robust solution outperforms 85.3% of the solutions while the deterministic solution outperforms only  
 382 about 1% of the solutions; for pollution, the deterministic solution outperforms 96% of the solutions  
 383 while the robust solution outperforms only 39.6% of the solutions. According to the ratio of  
 384  $SRI(Rob)/SRI(Det)$ , the deterministic solution is about 130% more uncertain than the robust solution  
 385 for water deficit; for pollution, the robust solution is about 37.7% more variable than the deterministic  
 386 solution. The distance of each solution to the origin can reflect the comprehensive performance of the  
 387 robustness of each solution. For the robustness composite index, the ratio of  $Dis(Rob)/Dis(Det)$  is  
 388 0.655, which means that the composite robustness of the robust solution is 52.6% higher than the  
 389 robustness of the deterministic solution.

390 For the robustness composite, the robust solution outperforms all the solutions, while the deterministic  
 391 model solution outperforms only about 3.2% of the solutions. Comparing the distance to the origin of  
 392 the robust solution and the deterministic solution, we can find that the robustness of the robust solution  
 393 improves by 27.8% over the deterministic solution.

394 **4.6 Analysis of specific water resources allocation schemes**

395 First, as shown in Figure 13, we analyzed the proportion of water supply for each city. We find that the  
 396 water supply share for the scheme most robust to water deficit rates is significantly higher than that for  
 397 the scheme with the most robust pollutant emissions. This is because an increase in water supply leads  
 398 to an increase in pollutant emissions, which in turn leads to a decrease in the robustness of pollutant  
 399 emissions. For specific cities, the least robust allocation scenario for water deficit reduces the water  
 400 supply in City 3, City 7, City 10, City 12, and City 15 compared to the most robust allocation scenario  
 401 for pollutant emissions. Interestingly, these cities have the most water demand in the basin (as shown in  
 402 Figure 3). Therefore, basin managers can increase the water supply to these cities if they need to improve  
 403 the water deficit robustness of the water resources allocation scheme.

404 Then we analyze specifically the distribution of water resources between sectors. An interesting  
 405 phenomenon can be observed. As shown in Figure 13, although the scenario with the best robustness in  
 406 terms of pollutant emissions has a lower water supply than the scenario with the best robustness in terms  
 407 of water deficit, the reduction is mainly in the agricultural sector. Water for domestic and industrial  
 408 production did not change much. The reason for this may be that agricultural water use causes more  
 409 pollution and may create more uncertainty. So how can watershed managers hope that improving the  
 410 robustness of pollutant discharge can reduce water supply to the agricultural sector.



411  
 412 **Figure 13.** Specific water resources allocation schemes.

413 **5. Conclusion**

414 In this study, we propose a multi-objective robustness analysis method considering multiple uncertainties  
 415 (CM-ROPAR approach) based on the robust optimization method for uncertainty perception (ROPAR  
 416 approach). To verify the superiority and practicality of the CM-ROPAR approach, four robustness criteria  
 417 are selected, and we compare the robust solution calculated by the method with the optimal solution of  
 418 the deterministic model. In the studied case, there is a competitive relationship between the robustness  
 419 of the two objective functions, which can form a Pareto frontier. For the water deficit rate, the robust  
 420 solution outperforms the deterministic solution by 53%, 59%, 162%, and 1167% for the four robustness  
 421 criteria, respectively; for the pollutant emission, the deterministic solution outperforms the robust



422 solution by only 17% for *RC1 – RC3*, and outperforms the robust solution by 137% for *RC4*. For the  
423 composite robustness, the robust solution outperforms the deterministic solution by 52.6%, the CM-  
424 ROPAR finds a more robust solution.

425 The CM-ROPAR approach permits to exhibit the handling of uncertainty, to be able to analyze how  
426 uncertainty is transmitted to the Pareto frontier, and to perform the corresponding probabilistic analysis.  
427 The novelty of the new method compared to existing ROPAR methods is reflected in two aspects. First,  
428 the ROPAR method only considers uncertainty at a single point. In contrast, the CM-ROPAR method  
429 considers multiple uncertainties through the joint probability distribution of two points, which is closer  
430 to the actual situation and more general. Second, the new way analyzes the robustness of two objective  
431 functions of the solution instead of fixing one objective function to analyze the robustness of the other  
432 objective function. The CM-ROPAR method is more comprehensive and can identify the robustness of  
433 both objective functions, giving decision-makers more information for decision making.

434 One of the limitations of this study is that the CM-ROPAR approach is applicable to problems with  
435 two uncertainties and two objective functions; however, water allocation allows for more uncertainties  
436 and more objective functions (e.g., the uncertainty of inflow between multiple tributaries). In future  
437 research, we will focus on more complex objective functions and multi-objective optimization problems  
438 with at least three objective functions.

439

440 *Author contribution.* JZ and DS conceptualized the study and wrote the paper. ZD provided the data. All  
441 the authors took part in the interpretation of the results and edits of the paper.

442

443 *Competing interests.* The authors declare that they have no conflict of interest.

444

445 *Acknowledgements.* This research has been supported by the

446

## 447 **Reference**

448 Abdulkaki, D., Al-Hindi, M., Yassine, A., and Abou Najm, M.: An optimization model for the allocation  
449 of water resources, *Journal of Cleaner Production*, 164, 994-1006, 10.1016/j.jclepro.2017.07.024, 2017.

450 Ashofteh, P. S., Haddad, O. B., and A. Mariño, M.: Climate Change Impact on Reservoir Performance  
451 Indexes in Agricultural Water Supply, *Journal of Irrigation and Drainage Engineering*, 139, 85-97,  
452 10.1061/(asce)ir.1943-4774.0000496, 2013.

453 Beyer, H.-G. and Sendhoff, B.: Robust optimization – A comprehensive survey, *Computer Methods in*  
454 *Applied Mechanics and Engineering*, 196, 3190-3218, 10.1016/j.cma.2007.03.003, 2007.

455 Chen, L., Xu, L., and Yang, Z.: Accounting carbon emission changes under regional industrial transfer  
456 in an urban agglomeration in China's Pearl River Delta, *Journal of Cleaner Production*, 167, 110-119,  
457 10.1016/j.jclepro.2017.08.041, 2017.

458 Dong, Y. and Xu, L.: Aggregate risk of reactive nitrogen under anthropogenic disturbance in the Pearl  
459 River Delta urban agglomeration, *Journal of Cleaner Production*, 211, 490-502,  
460 10.1016/j.jclepro.2018.11.194, 2019.

461 Habibi Davijani, M., Banihabib, M. E., Nadjafzadeh Anvar, A., and Hashemi, S. R.: Multi-Objective  
462 Optimization Model for the Allocation of Water Resources in Arid Regions Based on the Maximization  
463 of Socioeconomic Efficiency, *Water Resources Management*, 30, 927-946, 10.1007/s11269-015-1200-y,  
464 2016.

465 Hassanzadeh, E., Elshorbagy, A., Wheeler, H., and Gober, P.: A risk-based framework for water resource

466 management under changing water availability, policy options, and irrigation expansion, *Advances in*  
467 *Water Resources*, 94, 291-306, 10.1016/j.advwatres.2016.05.018, 2016.

468 Jin, S. W., Li, Y. P., Yu, L., Suo, C., and Zhang, K.: Multidivisional planning model for energy, water and  
469 environment considering synergies, trade-offs and uncertainty, *Journal of Cleaner Production*, 259,  
470 10.1016/j.jclepro.2020.121070, 2020.

471 Kang, D. and Lansey, K.: Scenario-Based Robust Optimization of Regional Water and Wastewater  
472 Infrastructure, *Journal of Water Resources Planning and Management*, 139, 325-338,  
473 10.1061/(asce)wr.1943-5452.0000236, 2013.

474 Kapelan, Z., Savic, D. A., Walters, G. A., and Babayan, A. V.: Risk- and robustness-based solutions to a  
475 multi-objective water distribution system rehabilitation problem under uncertainty, *Water Sci Technol*,  
476 53, 61-75, 10.2166/wst.2006.008, 2006.

477 Kapelan, Z. S., Savic, D. A., and Walters, G. A.: Multiobjective design of water distribution systems  
478 under uncertainty, *Water Resources Research*, 41, 10.1029/2004wr003787, 2005.

479 Keath, N. A. and Brown, R. R.: Extreme events: being prepared for the pitfalls with progressing  
480 sustainable urban water management, *Water Sci Technol*, 59, 1271-1280, 10.2166/wst.2009.136, 2009.

481 Li, M., Fu, Q., Singh, V. P., Liu, D., and Gong, X.: Risk-based agricultural water allocation under multiple  
482 uncertainties, *Agricultural Water Management*, 233, 10.1016/j.agwat.2020.106105, 2020.

483 Lu, H., Ren, L., Chen, Y., Tian, P., and Liu, J.: A cloud model based multi-attribute decision making  
484 approach for selection and evaluation of groundwater management schemes, *Journal of Hydrology*, 555,  
485 881-893, 10.1016/j.jhydrol.2017.10.009, 2017.

486 Ma, Y., Li, Y. P., and Huang, G. H.: A bi-level chance-constrained programming method for quantifying  
487 the effectiveness of water-trading to water-food-ecology nexus in Amu Darya River basin of Central Asia,  
488 *Environ Res*, 183, 109229, 10.1016/j.envres.2020.109229, 2020.

489 Marchi, A., Dandy, G. C., and Maier, H. R.: Integrated Approach for Optimizing the Design of Aquifer  
490 Storage and Recovery Stormwater Harvesting Schemes Accounting for Externalities and Climate Change,  
491 *Journal of Water Resources Planning and Management*, 142, 10.1061/(asce)wr.1943-5452.0000628,  
492 2016.

493 Marquez Calvo, O. O., Quintiliani, C., Alfonso, L., Di Cristo, C., Leopardi, A., Solomatine, D., and de  
494 Marinis, G.: Robust optimization of valve management to improve water quality in WDNs under demand  
495 uncertainty, *Urban Water Journal*, 15, 943-952, 10.1080/1573062x.2019.1595673, 2019.

496 Nelsen, R. B., Quesada-Molina, J. J., Rodríguez-Lallena, J. A., and Úbeda-Flores, M.: On the  
497 construction of copulas and quasi-copulas with given diagonal sections, *Insurance: Mathematics and*  
498 *Economics*, 42, 473-483, 10.1016/j.insmatheco.2006.11.011, 2008.

499 Nikoo, M. R., Kerachian, R., Karimi, A., and Azadnia, A. A.: Optimal water and waste-load allocations  
500 in rivers using a fuzzy transformation technique: a case study, *Environ Monit Assess*, 185, 2483-2502,  
501 10.1007/s10661-012-2726-6, 2013.

502 Quintiliani, C., Marquez-Calvo, O., Alfonso, L., Di Cristo, C., Leopardi, A., Solomatine, D. P., and de  
503 Marinis, G.: Multiobjective Valve Management Optimization Formulations for Water Quality  
504 Enhancement in Water Distribution Networks, *Journal of Water Resources Planning and Management*,  
505 145, 10.1061/(asce)wr.1943-5452.0001133, 2019.

506 Reed, P. M., Hadka, D., Herman, J. D., Kasprzyk, J. R., and Kollat, J. B.: Evolutionary multiobjective  
507 optimization in water resources: The past, present, and future, *Advances in Water Resources*, 51, 438-  
508 456, 10.1016/j.advwatres.2012.01.005, 2013.

509 Ren, C., Li, Z., and Zhang, H.: Integrated multi-objective stochastic fuzzy programming and AHP

510 method for agricultural water and land optimization allocation under multiple uncertainties, *Journal of*  
511 *Cleaner Production*, 210, 12-24, 10.1016/j.jclepro.2018.10.348, 2019.

512 Solomatine, D.: An approach to multi-objective robust optimization allowing for explicit analysis of  
513 robustness, <https://www.un-ihe.org/sites/default/files/solomatine-ropar.pdf>, 2012.

514 Solomatine, D. P. and Marquez-Calvo, O. O.: Approach to robust multi-objective optimization and  
515 probabilistic analysis: the ROPAR algorithm, *Journal of Hydroinformatics*, 21, 427-440,  
516 10.2166/hydro.2019.095, 2019.

517 Sun, S., Fu, G., Bao, C., and Fang, C.: Identifying hydro-climatic and socioeconomic forces of water  
518 scarcity through structural decomposition analysis: A case study of Beijing city, *Sci Total Environ*, 687,  
519 590-600, 10.1016/j.scitotenv.2019.06.143, 2019.

520 Xiong, W., Li, Y., Pfister, S., Zhang, W., Wang, C., and Wang, P.: Improving water ecosystem  
521 sustainability of urban water system by management strategies optimization, *J Environ Manage*, 254,  
522 109766, 10.1016/j.jenvman.2019.109766, 2020.

523 Xu, Z., Pan, B., Han, M., Zhu, J., and Tian, L.: Spatial-temporal distribution of rainfall erosivity, erosivity  
524 density and correlation with El Niño-Southern Oscillation in the Huaihe River Basin, China, *Ecological*  
525 *Informatics*, 52, 14-25, 10.1016/j.ecoinf.2019.04.004, 2019.

526 Yang, W., Li, X., Sun, T., Pei, J., and Li, M.: Macrobenthos functional groups as indicators of ecological  
527 restoration in the northern part of China's Yellow River Delta Wetlands, *Ecological Indicators*, 82, 381-  
528 391, 10.1016/j.ecolind.2017.06.057, 2017.

529 Yazdi, J., Lee, E. H., and Kim, J. H.: Stochastic Multiobjective Optimization Model for Urban Drainage  
530 Network Rehabilitation, *Journal of Water Resources Planning and Management*, 141,  
531 10.1061/(asce)wr.1943-5452.0000491, 2015.

532 Yu, S. and Lu, H.: An integrated model of water resources optimization allocation based on projection  
533 pursuit model – Grey wolf optimization method in a transboundary river basin, *Journal of Hydrology*,  
534 559, 156-165, 10.1016/j.jhydrol.2018.02.033, 2018.

535 Zeng, X., Zhao, J., Wang, D., Kong, X., Zhu, Y., Liu, Z., Dai, W., and Huang, G.: Scenario analysis of a  
536 sustainable water-food nexus optimization with consideration of population-economy regulation in  
537 Beijing-Tianjin-Hebei region, *Journal of Cleaner Production*, 228, 927-940,  
538 10.1016/j.jclepro.2019.04.319, 2019.

539 Zhu, F., Zhong, P.-a., Cao, Q., Chen, J., Sun, Y., and Fu, J.: A stochastic multi-criteria decision making  
540 framework for robust water resources management under uncertainty, *Journal of Hydrology*, 576, 287-  
541 298, 10.1016/j.jhydrol.2019.06.049, 2019.

542 Zhuang, X. W., Li, Y. P., Nie, S., Fan, Y. R., and Huang, G. H.: Analyzing climate change impacts on  
543 water resources under uncertainty using an integrated simulation-optimization approach, *Journal of*  
544 *Hydrology*, 556, 523-538, 10.1016/j.jhydrol.2017.11.016, 2018.

545